ity of the soft-landed PKAc was estimated on the basis of the phosphorylation assay (Fig. 5) and estimated ion currents. This rough estimate gave values of ~50% of the specific activity of the original enzyme preparation in several different experiments. In this series of experiments sensitive, intracellular enzymes were ionized by electrospray under mild conditions (physiological pH, aqueous media), and mass-selected multiply charged ions were transferred to another hydrophilic medium represented by the glycerol liquid surface. The fact that these kinases survived this process and retained their biological activity is evidence that soft-landing of active enzymes is feasible for various eukaryotic (e.g., human) cytosolic proteins.

Mass spectrometry represents a separation method that is complementary to chromatography or electrophoresis. Traditional methods may fail to separate species having highly similar structures, but mass spectrometry should be successful as long as the molecular weights are different. Although the ionization of complex protein mixtures can suffer from suppression effects (*26*) in either ESI or MALDI, these will be minimized when the analytes are highly similar, as in the case of mixtures of synthetic (*27*) and biological (*15*) polymer congeners like polyclonal antibodies, glycoproteins, and polysulfonated or phosphorylated products of posttranslational modification. Collection of "fractions" in a soft-landing experiment can be performed easily, by moving either the target (as demonstrated) or the ion beam on the surface to yield an array of the separated components of the initial mixture. These arrays could also provide tools for combinatorial chemistry–based methods, like identification of target molecules (*28*).

References and Notes

1. M. Schena, D. Shalon, R. W. Davis, P. O. Brown, *Science* **270**, 467 (1995).
2. C. A. Rowe, S. B. Scruggs, M. J. Feldstein, J. P. Golden, F. S. Ligler, *Anal. Chem.* **71**, 433 (1999).
3. J. F. Mooney *et al.*, *Proc. Natl. Acad. Sci. U.S.A.* **93**, 12287 (1996).
4. V. W. Jones, J. R. Kenseth, M. D. Porter, C. L. Mosher, E. Henderson, *Anal. Chem.* **70**, 1233 (1998).
5. T. Laurell, L. Wallman, J. J. Nilsson, *Micromech. Microeng.* **9**, 369 (1999).
6. V. N. Morozov, T. Y. Morozova, *Anal. Chem.* **71**, 3110 (1999).
7. G. MacBeath, S. L. Schreiber, *Science* **289**, 1760 (2000).
8. B. D. Martin, B. P. Gaber, C. H. Patterson, D. C. Turner, *Langmuir* **14**, 3971 (1998).
9. A. Roda, M. Guardigli, C. Russo, P. Pasini, M. Baraldini, *Biotechniques* **28**, 492 (2000).
10. R. G. Cooks, Z. Ouyang, application for U.S. Patent.
11. V. Franchetti, B. H. Solka, W. E. Baitinger, J. W. Amy, R. G. Cooks, *Int. J. Mass Spectrom. Ion Phys.* **23**, 29 (1977).
12. S. A. Miller, H. Luo, S. Pachuta, R. G. Cooks, *Science* **275**, 1447 (1997).
13. H. Luo, S. A. Miller, R. G. Cooks, S. J. Pachuta, *Int. J. Mass Spectrom. Ion Processes* **174**, 193 (1998).
14. R. J. Geiger, M. C. Melnyk, K. L. Busch, M. G. Bartlett, *Int. J. Mass Spectrom. Ion Processes* **182/183**, 415 (1999).
15. B. Feng, D. S. Wunschel, C. D. Masselon, L. Pasa-Tolic, R. D. Smith, *J. Am. Chem. Soc.* **121**, 8961 (1999).
16. K. Bromann *et al.*, *Science* **274**, 956 (1996).
17. S. D. Fuerstenau *et al.*, *Angew. Chem. Int. Ed.* **40**, 541 (2001).
18. A four-protein mixture of apomyoglobin, cytochrome c, insulin, and lysozyme (0.0025 mg/ml each) in 1% acetic acid in 1:1 MeOH:H_2O (v/v) was used for soft-landing of the four-spot array. Proteins were obtained from Sigma (St. Louis, MO).
19. Various surfaces, including aluminum, gold, various functionalized SAM surfaces, and some liquid surfaces, have been used as substrates for ion soft-landing. The data shown in this report are for gold and various liquids.
20. Details of protein-purification methods and of the bioassays performed are available on *Science* Online.
21. J. C. Schwartz, M. Senko, *J. Am. Soc. Mass Spectrom.* **13**, 659 (2002).
22. MALDI sample preparation was carried out by applying 1 μl of saturated sinapinic acid solution in 0.1% aqueous trifluoroacetic acid/acetonitrile 2:1 onto the landed material. The dried sample was analyzed with a Bruker Reflex III instrument, in the positive ion mode, with delayed extraction. Singly and doubly protonated ions of lysozyme, cytochrome c, and apomyoglobin were detected in the linear mode.
23. Characteristic fragments of lysozyme were detected on the surface by MALDI in the case of COOH-terminated SAM at 10 eV/charge collision energy.
24. J. C. Lee, S. N. Timasheff, *J. Biol. Chem.* **256**, 7193 (1981).
25. We carried out blank experiments by isolating and landing ions from regions of the mass spectrum that did not contain the ionized proteins of interest while continuing to perform protein ionization; no phosphorylation was detected for either enzyme.
26. P. Pan, S. A. McLuckey, *Anal. Chem.* **75**, 1491 (2003).
27. G. Siuzdak, T. Hollenbeck, B. Bothner, *J. Mass Spectrom.* **34**, 1087 (1999).
28. H. Zhu, M. Snyder, *Curr. Opin. Chem. Biol.* **7**, 55 (2003).

29. This work was supported by the Indiana Proteomics Consortium. We acknowledge helpful discussions with R. DiMarchi, J. Hale, J. Hurrell, M. Knierman, R. Ludwig, P. Pan, M. Senko, J. LaDine, and I. Jardine.

Supporting Online Material

www.sciencemag.org/cgi/content/full/1088776/DC1
Methods
Figs. S1 to S3

3 July 2003; accepted 5 August 2003
Published online 14 August 2003;
10.1126/science.1088776
Include this information when citing this paper.

Simultaneous Fluorescence and Raman Scattering from Single Carbon Nanotubes

Achim Hartschuh,[1,3] Hermeneglido N. Pedrosa,[2] Lukas Novotny,[1] Todd D. Krauss[2]

Single-molecule fluorescence spectroscopy was used to determine the electronic properties of individual single-walled carbon nanotubes. Carbon nanotube structure was determined simultaneously from Raman spectroscopy. Fluorescence spectra from individual nanotubes with identical structures have different emission energies and linewidths that likely arise from defects or the local environment. Unlike most other molecules studied to date, the fluorescence intensity or spectrum from a single nanotube unexpectedly did not fluctuate.

Single-walled carbon nanotubes (SWNTs) are synthesized as mixtures of metallic and semiconducting tubes (*1*). Their individual structures can be characterized by two integers [(*n*,*m*)] that define both their diameter and chirality (*2*); if ($n - m$) is not divisible by 3, the nanotubes are semiconducting. Recently, the photoluminescence of SWNT mixtures suspended in surfactant micelles in water was characterized as arising from band-gap fluorescence from semiconducting tubes with different structures (*3*, *4*). Such a spectrum (Fig. 1A) (*5*) contains overlapping fluorescence features. However, ensemble averaging obscures the true spectral linewidths and the details of the band shape. These optical properties are likely needed for the development of SWNT photonic applications, such as nanometer-scale, integrated electroluminescent devices (*6*).

[1]The Institute of Optics, [2]Department of Chemistry, University of Rochester, Rochester, NY 14627, USA. [3]Physikalische Chemie, Universität Siegen, 57068 Siegen, Germany.

We measured the electronic structure of individual SWNTs using single-molecule photoluminescence spectroscopy. Although the spectra from individual SWNTs with identical diameters were similar, they exhibited a distribution of peak positions and linewidths not observed in ensemble studies of isolated SWNTs (*3*, *4*, *7*). Unlike most single molecules (*8*) or semiconductor nanoparticles (*9*), the fluorescence for SWNTs does not show any spectral or intensity fluctuations.

Spatially isolated individual SWNTs were achieved by spin-coating ~75 μl of the SWNT suspension onto a glass coverslip (*5*). Fluorescent samples are known to contain short (~200 nm long) SWNTs isolated in micelles (*3*). Thus, we expected the spin-coating procedure to result in single SWNTs well dispersed on a thin surfactant layer. Indeed, atomic force microscopy measurements revealed predominantly short SWNTs (with lengths of 200 to 300 nm) on top of residual surfactant patches a few nanometers thick. Optical characterization of SWNT coverage was achieved through confo-

cal Raman imaging (*10*, *11*) and indicated a density of ~10 to 20 Raman-active nanotubes per 100 μm^2. Laser excitation at 633 nm ensured a spectral isolation of all Raman signals, which occur between 633 and 770 nm, from the fluorescence signals above 850 nm.

Figure 1B shows three fluorescence images of the same sample area, representing the collected number of photons at every pixel within the spectral windows marked in Fig. 1A. All images show distinct bright spots at different positions, indicating isolated emission sources with different emission energies. Figure 2A displays representative spectra detected at these bright spots for the three wavelength regions marked in Fig. 1. Each spectrum exhibits a single fluorescence band with a smooth line shape. The three spectra have emission maxima at wavelengths of 1016, 955, and 914 nm, respectively, which match three transitions observed in the ensemble spectrum (Fig. 1A).

Low-energy Raman features that correspond to scattering from the radial breathing mode (RBM) were used to verify that the observed emissions were from individual SWNTs. Raman spectra (Fig. 2B) were detected at identical sample positions (noted in Fig. 2 as 1, 2, and 3) as those used to obtain the fluorescence spectra in Fig. 2A. The frequency of the RBM (ω, in cm^{-1}) directly reflects the diameter of the SWNT (*D*, in nm), through $\omega = (223.5/D) + 12.5$ (*4*, *12*), and can be used to uniquely identify the structural parameters (*n*,*m*) (*13*). For all three sample positions, only one RBM peak (corresponding to the same individual SWNT) was observed within the instrument-limited linewidth of 10 cm^{-1}.

The observed emission energies and corresponding RBM frequencies are listed in Table 1, along with values obtained from fluorescence of ensemble samples (*4*). Nanotubes with emission beyond ~1030 nm will not be observed with our detector (Si CCD); thus, we can compare single nanotube fluorescence and Raman RBM data sets to ensemble data sets for a subset of all possible nanotube structures (Table 1). The mean measured fluorescence energy for a given SWNT structure (supporting online text), for resonant and nonresonant excitation, matches very well with ensemble fluorescence data sets (resonant excitation), confirming the assignment made by Bachilo *et al.* (*4*). We were not able to obtain resonance Raman data for (6,5) or (6,4) SWNTs, because the excitation energy (633 nm) was too small to populate the second excited state.

Single nanotube spectroscopy allows for a more detailed investigation of crucial SWNT optical and electronic properties without ensemble averaging. Emission spectra (Fig. 2A) show a single, featureless, symmetrical band that is very well described by a single Lorentzian line-shape function (Fig. 2A, solid lines) with a room-temperature broadened linewidth of approximately 23 meV (supporting online text). This agrees with the approximately 25-meV linewidths reported by O'Connell *et al.* (*3*). The absence of phonon sidebands that correspond to either the RBM (37 meV) or the tangential mode (197 meV) indicates a relatively weak electron-phonon coupling, in agreement with the weak coupling determined by ultrafast optical studies (*14*).

The correlation between emission and Raman signals can be further shown by variation of the excitation polarization. We detected the intensity of the Raman signal (the G band was at 1592 cm^{-1}) and the emission intensity simultaneously for individual SWNTs as a function of (linear) polarization direction. Both Raman and fluorescence signal intensities (*I*) show the same 180° periodicity (Fig. 3, A and B) that can be ascribed to the scalar product of the light polarization *P* and the transition dipole moment μ, because $I \sim |P(\theta) \bullet \mu|^2 = P\mu\cos^2\theta$, where θ is the angle between *P* and μ. Because the emission and Raman intensities exhibit essentially the same polarization dependence (to within an experimental error of 3°), the contributing transition dipole moments must have the same orientation. Polarized absorption measurements on SWNTs aligned in channels of single crystals and within nanotube yarns show the strongest absorption for light polarized parallel to the nanotube axis (*15*, *16*). Maximum signal intensities for resonant Raman scattering are also observed when nanotubes are aligned parallel to the polarization of the incident laser light (*17*), because of resonance enhancement.

The identical polarization dependence between fluorescence and Raman signals could possibly arise from a small bundle of SWNTs with identical structural parameters (*n*,*m*) and orientations. However, this possibility is extremely unlikely given (i) there is a large variety of potential nanotube structures and (ii) the solubilization procedure produces isolated SWNTs (*3*). Thus, the identical polarization dependence provides strong evidence of fluorescence from single nanotubes.

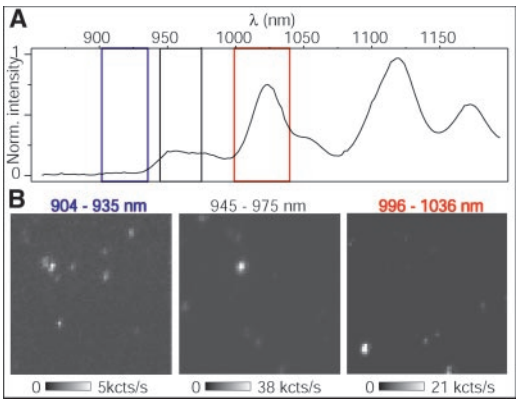

Fig. 1. Fluorescence images and spectra from isolated SWNTs. (**A**) Fluorescence spectrum between 850 and 1200 nm for a macroscopic sample of a SWNT suspension in D_2O after laser excitation at 633 nm. Vertical lines mark spectral windows where strong emission signals are expected. (**B**) Confocal fluorescence images (10 μm by 10 μm) of single spatially isolated SWNTs on glass, acquired by raster scanning of the sample and simultaneous detection of an optical spectrum at every pixel (*5*). Spectroscopic images were obtained by integration of the detected intensities within the spectral windows in (A). Norm., normalized; kcts, kilocounts.

Table 1. Spectral data and structural assignments for SWNTs. λ_{Em} is the measured average emission wavelength. $h\nu_{Em}$ is the measured average emission energy (supporting online text); the literature values (lit.) were obtained from (*4*). ν_{RBM} is the RBM frequency. Superscripts correspond to the spectra (1, 2, and 3) marked in Fig. 2. –, Raman spectra were not observed because the excitation energy was nonresonant.

λ_{Em} (nm)	$h\nu_{Em}$ (eV)	$h\nu_{Em}$ (lit.) (eV)	Observed $\nu_{RBM} \pm 5$ (cm^{-1})	Predicted ν_{RBM} (cm^{-1})	(*n*,*m*) structure
1023	1.212 (1.220[1])	1.212	286[1]	281.9	(7,5)
976	1.270	1.272	–	307.4	(6,5)
955	1.298 (1.298[2])	1.302	296[2]	298.1	(8,3)
915	1.355 (1.357[3])	1.359	309[3]	307.4	(9,1)
881	1.407	1.420	–	335.2	(6,4)

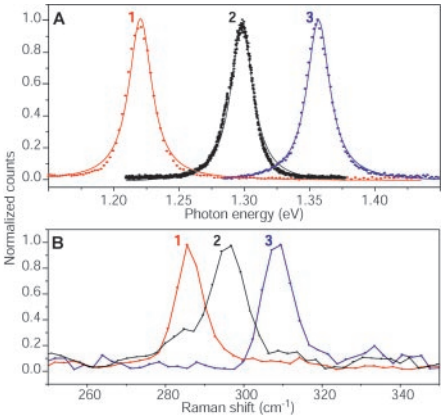

Fig. 2. Fluorescence and Raman spectra of single SWNTs. (**A**) Fluorescence spectra were detected for three different sample positions, labeled 1 to 3. Solid lines are fits with single Lorentzian line-shape functions. (**B**) Raman spectra obtained from the positions described in (A). The Raman shift corresponds to scattering from the nanotube RBM.

Time traces of the single SWNT fluorescence intensity recorded with moderate excitation intensities (<70 kW/cm^{-2}) show a constant amplitude over many seconds, with no indication of fluctuations on a time scale of 40 ms to 100 s (Fig. 3C). This absence of spectral and intensity fluctuations is in stark contrast to fluorescence from individual semiconductor quantum dots (*9*) and from most molecules (*8*), which exhibit an emission intermittency or on-off blinking behavior for all excitation intensities on time scales that span many orders of magnitude (*18*). At higher excitation powers, SWNT fluorescence intensity fluctuations can be observed that are likely due to laser-induced sample heating. The observation that SWNTs show no emission intensity blinking or bleaching demonstrates that SWNTs have the potential to provide a stable, single-molecule infrared photon source with extremely narrow linewidth.

Simultaneous resonance Raman and fluorescence measurements also revealed that the emission characteristics for a SWNT with a given (*n*,*m*) are not uniform. Although Raman spectra (including RBM frequencies) were identical, indicating SWNTs with the same (*n*,*m*) structure, in some cases the corresponding emission spectra were considerably different (Fig. 4). SWNTs with the same (*n*,*m*) showed a distribution of emission energies centered at the energies listed in Table 1, as well as a distribution of linewidths (supporting online text). Spectra that deviated from the energies listed in Table 1 were often accompanied by asymmetric, broad linewidths (up to 50 meV) and weaker fluorescence intensities when compared to those of the Lorentzian-shaped bands. Structural (*19*) or chemical defects as well as fluctuations in the local environment, such as electrostatic surface potential changes (*20*) or localized charges (*21*), can perturb the electronic band structure of SWNTs. Because of the strong correlation between SWNT electronic configuration (and hence optical emission) and structure or local environment, we attribute the nonuniform emission properties to these localized defects and perturbations.

Studies of SWNT mixtures (*4*) have determined that for larger nanotubes the ratio of the second excited state energy to the fluorescence energy approaches 1.75. However, according to one-electron theories, one would expect a ratio of 2. This deviation was recently proposed to arise from strong electron-hole interactions for carriers excited into the second excited state only (*22*). For (6,4) or (6,5) nanotubes pumped into the first excited state, the fluorescence energy is the same as that found when the second excited state was populated (*4*). Thus, our data, although limited to small-diameter nanotubes, do not support a strong electron-hole interaction theory.

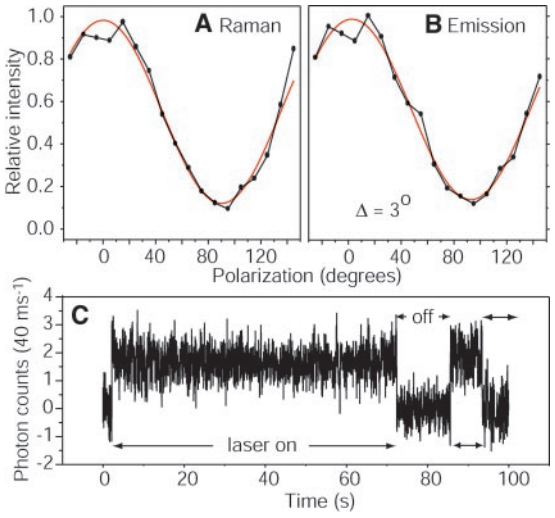

Fig. 3. Polarization and photon statistics of SWNT fluorescence. (**A** and **B**) Polarization dependence of (A) the resonant Raman (G-band) signal and (B) the fluorescence signal for a single SWNT. The red curves are fits that assume a $\cos^2\theta$ dependence, where θ is the relative angle of rotation of the excitation polarization. $\Delta = 3°$ is the phase shift between the relative intensity of the Raman and fluorescence signals. (**C**) Time trace of an emission signal in intervals of 40 ms. The excitation was physically blocked during the "off" periods (*11*).

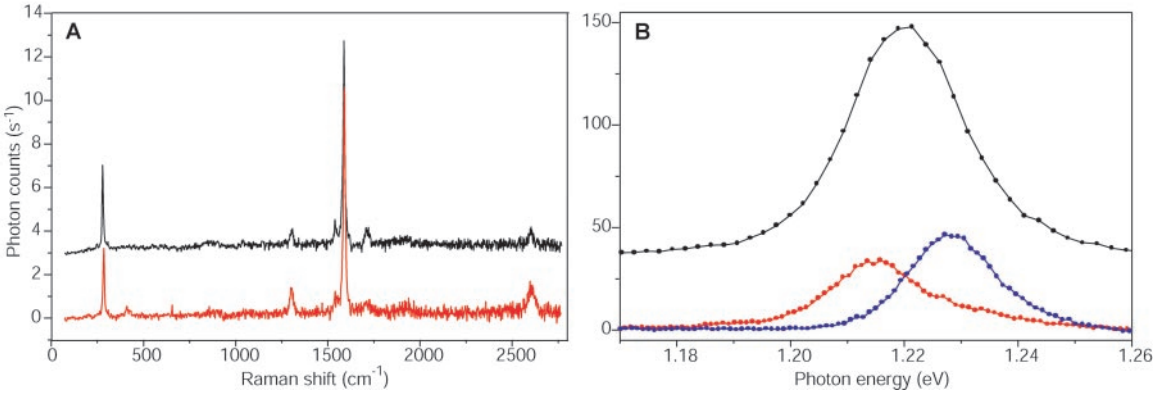

Fig. 4. Correlated Raman and fluorescence spectra. (**A**) Resonance Raman spectra for individual SWNTs at different sample positions (different SWNTs). The identical Raman spectra indicate these SWNTs have the same (7,5) structure. The spectra are offset for clarity, and the Raman spectrum corresponding to the blue emission spectrum in (B) is also omitted for clarity. (**B**) Fluorescence spectra for three individual SWNTs at positions that correspond to those in (A). The spectral position, amplitude, and shape of the fluorescence bands differ substantially. The spectra are offset for clarity.

References and Notes

1. C. Journet *et al.*, *Nature* **388**, 756 (1997).
2. R. Saito, G. Dresselhaus, M. S. Dresselhaus, *Physical Properties of Carbon Nanotubes* (Imperial College Press, London, 1998).
3. M. J. O'Connell *et al.*, *Science* **297**, 593 (2002).
4. S. M. Bachilo *et al.*, *Science* **298**, 2361 (2002).
5. Materials and methods are available as supporting material on *Science* Online.
6. J. A. Misewich *et al.*, *Science* **300**, 783 (2003).
7. S. Lebedkin, F. Hennrich, T. Skipa, M. M. Kappes, *J. Phys. Chem. B* **107**, 1949 (2003).
8. J. K. Trautman, J. J. Macklin, L. E. Brus, E. Betzig, *Nature* **369**, 40 (1994).
9. M. Nirmal *et al.*, *Nature* **383**, 802 (1996).
10. A. Hartschuh, E. J. Sánchez, X. S. Xie, L. Novotny, *Phys. Rev. Lett.* **90**, 95503 (2003).
11. J. Zhao *et al.*, *Nano Lett.* **2**, 823 (2002).
12. A. M. Rao *et al.*, *Science* **275**, 187 (1997).
13. A. Jorio *et al.*, *Phys. Rev. Lett.* **86**, 1018 (2001).
14. T. Hertel, G. Moos, *Phys. Rev. Lett.* **84**, 5002 (2000).
15. Z. M. Li *et al.*, *Phys. Rev. Lett.* **87**, 127401 (2001).
16. K. Jiang, Q. Li, S. Fan, *Nature* **419**, 801 (2002).
17. G. S. Duesberg, I. Loa, M. Burghard, K. Syassen, S. Roth, *Phys. Rev. Lett.* **85**, 5436 (2000).
18. W. E. Moerner, M. Orrit, *Science* **283**, 1670 (1999).
19. T. W. Tombler *et al.*, *Nature* **405**, 769 (2000).
20. M. T. Woodside, P. L. McEuen, *Science* **296**, 1098 (2002).
21. P. L. McEuen, M. Bockrath, D. H. Cobden, Y. G. Yoon, S. G. Louie, *Phys. Rev. Lett.* **83**, 5098 (1999).
22. C. L. Kane, E. J. Mele, *Phys. Rev. Lett.* **90**, 2074011 (2003).

23. Supported by the Research Corporation (grant no. R-10733), the New York State Office of Science and Academic Research (grant no. C-020085), the Department of Energy (grant no. DE-FG02-01ER15204), and the National Science Foundation (grant no. BES-0086368).

Supporting Online Material

www.sciencemag.org/cgi/content/full/301/5638/1354/DC1
Materials and Methods
SOM Text
Fig. S1
References and Notes

22 May 2003; accepted 4 August 2003